Improvement of magnetoresistance over a wide temperature range in $La_{2/3}Sr_{1/3}MnO_3$/polymer composites

2002 J. Phys.: Condens. Matter 14 9607

(http://iopscience.iop.org/0953-8984/14/41/316)

INSTITUTE OF PHYSICS PUBLISHING JOURNAL OF PHYSICS: CONDENSED MATTER

J. Phys.: Condens. Matter **14** (2002) 9607–9614 PII: S0953-8984(02)39003-9

Improvement of magnetoresistance over a wide temperature range in $La_{2/3}Sr_{1/3}MnO_3$/polymer composites

Chun-Hua Yan[1], **Yun-Hui Huang**[2], **Xing Chen, Chun-Sheng Liao and Zhe-Ming Wang**

State Key Laboratory of Rare Earth Materials Chemistry and Applications, PKU-HKU Joint Laboratory in Rare Earth Materials and Bio-inorganic Chemistry, College of Chemistry and Molecular Engineering, Peking University, Beijing 100871, China

E-mail: chyan@chem.pku.edu.cn (Chun-Hua Yan)

Received 2 July 2002, in final form 28 August 2002
Published 4 October 2002
Online at stacks.iop.org/JPhysCM/14/9607

Abstract

Polymer-embedded $La_{2/3}Sr_{1/3}MnO_3$ (LSMO) composites, $(LSMO)_{1-x}(PPP)_x$ (PPP is polyparaphenylene, and x is the weight fraction of PPP), were prepared by mixing pre-prepared LSMO and PPP powders. Thermogravimetric analysis, x-ray diffraction, and infrared spectra show that the composites are stable when calcined at 400 °C. Significant enhancement in the magnetoresistance (MR) effect over a wide temperature range is observed for the composites compared with the parent LSMO. The MR enhancement reaches its maximum at $x = 0.2$. The magnetotransport is mainly attributed to intergrain spin-polarized tunnelling. We argue that the introduction of PPP gives rise to magnetic disorder and hence an enhanced tunnelling effect, which is responsible for the MR enhancement.

1. Introduction

Very recently, manganite-based two-phase composites have aroused substantial interest due to the improvement in their magnetoresistance (MR) near room temperature and/or under a low applied field, which holds promise for practical applications [1–4]. This improvement can be interpreted within the model of spin-polarized intergrain tunnelling proposed by Hwang *et al* [5]. On the basis of Hwang's model, adjusting the barrier layer by altering the size of the ferromagnetic grains or dilution with a nonmagnetic compound will significantly influence the tunnelling process and hence the MR. We have also observed enhanced MR in $La_{0.7}Sr_{0.3}MnO_3$-based composites with $CoFe_2O_4$, SiO_2, and $Sm_{0.7}Sr_{0.3}MnO_3$ [6–8]. Interestingly, embedding

[1] Author to whom any correspondence should be addressed.
[2] Present address: Institute of Advanced Materials and Technology, Fudan University, Shanghai 200433, China.

of some special phases, such as metallic silver [9] and superconducting $La_{1.85}Sr_{0.15}CuO_4$ [10], into the matrices of the manganite can produce upshift of the metal–insulator (M–I) transition temperature and negative–positive-tunable MR, respectively. Here, the second phase is important to the MR effect, but it is not very clear what kind of embedded compound is suitable for MR enhancement. Thus it is a challenge to find new composites with optimal MR properties.

It is well known that polymer compounds find extensive use in the preparation or property modification of inorganic materials. Many polymer/inorganic composites with novel properties have already been discovered and successfully used in various fields—such as battery cathodes, nonlinear optics, and sensors [11–13]. However, polymers used in combination with manganite oxides for CMR purposes have rarely been reported. In our previous work, we employed a distinctive conjugated polymer compound, polyparaphenylene (PPP), to fabricate $La_{2/3}Ca_{1/3}MnO_3$-based composites, and found a remarkable enhanced MR especially at low temperatures [14]. PPP has high thermal and oxidative stability. Because pure PPP is a good insulator, it can serve as a transport barrier in the manganite matrix to adjust the tunnelling effect and hence the MR. In addition, PPP can be modified from an insulator to an electrical conductor by a redox process, so we can conveniently control the interface conductivity for further investigation. In this paper, we introduced PPP into high-Curie-temperature $La_{2/3}Sr_{1/3}MnO_3$ (LSMO) to form LSMO/PPP composites to allow us to consider room temperature MR. A significant enhancement in MR over a wide temperature range was observed. The influence of the embedded PPP on the microstructure and magnetic and transport properties was also investigated.

2. Experimental details

PPP powders were synthesized using the Kovacic method through cationic polymerization of benzene [15, 16]. Aluminium chloride was used as a catalyst, and cupric chloride served as an oxidant. The reaction can be described as follows.

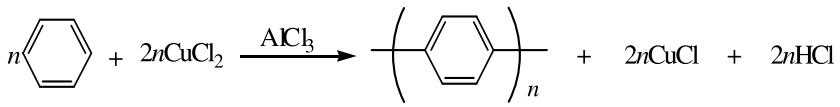

LSMO powders were prepared by thermal decomposition of complex precursors with $La(NO_3)_3{\cdot}6H_2O$, $Sr(NO_3)_2$, and $Mn(CH_3COO)_2{\cdot}4H_2O$ as initial reactants [17]. The powders obtained were preheated at 500 °C for 1 h, and then calcined at 1000 °C for another 1 h to achieve polycrystalline LSMO.

The composites $(LSMO)_{1-x}(PPP)_x$ (x is the weight fraction of PPP) were prepared by mixing pre-prepared LSMO and PPP powders in the appropriate ratios. The two precursor powders were mixed together, ground carefully in an agate mortar, and subsequently pressed into pellets 6 mm in diameter at a pressure of 0.25 ton mm^{-2}. Then the pellets were finally calcined at 400 °C for 1 h in air in order to make a good connection between adjacent LSMO and PPP particles.

The composition of LSMO was detected by an inductively coupled plasma atomic emission spectrometer (ICP, Leeman Lab. Inc.). Elemental analysis for PPP was carried out on a Perkin-Elmer 240C analyser. The thermogravimetric analysis (TGA) was performed using a commercial thermal analyser (Du Pont 2100) on 4–5 mg samples in air with a heating rate of 10 °C min^{-1}. The infrared spectra (FTIR) were measured by a Nicolet Magna 750 spectrometer. The phase was checked by an x-ray powder diffractometer (XRD, Rigaku, D_{max}-2000, Cu Kα radiation), and the morphology was probed by a scanning electronic microscope (SEM, 1910

FE, Amray). The magnetization and MR were obtained by a MagLab System 2000 (Oxford, UK). The resistance was measured using a standard four-probe technique from 5 to 310 K. The MR value was calculated as $(\rho_0 - \rho_H)/\rho_0$, where ρ_0 and ρ_H are the resistivity at zero field and under an applied field, respectively.

3. Results and discussion

Elemental analysis of PPP shows that the weight per cent is 93.4% for C and 5.2% for H, which is consistent with the theoretical value. From the micro-FTIR spectrum of PPP, we can observe three main characteristic bands centred at 806, 1000, and 1482 cm^{-1}, which are attributable to the C–H out-of-plane and in-plane vibrations of a para-substituted benzene ring and C=C skeletal in-plane vibration, respectively. The wavenumber of the C–H out-of-plane vibration band is tightly related to the degree of polymerization (n). When n increases, the band shifts to a lower wavenumber. Thus the value of n can be estimated according to the wavenumber [18]. For our case, n for PPP is between 15 and 30. Meanwhile, for the parent LSMO, the ICP result shows the same stoichiometry for La, Sr, and Mn, as expected, and iodometric titration indicates an Mn^{4+}/Mn ratio of 0.36 ± 0.02. XRD patterns indicate the formation of single-phase perovskite. The average particle size of LSMO is about 120 nm, as observed by SEM.

Figure 1 displays TGA curves of $(LSMO)_{1-x}(PPP)_x$ with $x = 0.2$, 0.6, and 1. It is found that the decomposition of pure PPP occurs at about 600 °C, which is indicative of a good thermal stability—whereas the initial combustion temperatures of PPP in the composites with $x = 0.2$ and 0.6 are about 420 and 450 °C respectively, both of which are lower than that of pure PPP. This may be due to a catalytic oxidation process in the composite promoted by Mn^{3+}/Mn^{4+} or atomic oxygen that has escaped from the LSMO lattice during calcining. However, the final calcining at 400 °C for the composite pellets does not lead to any other reaction between PPP and LSMO. This is further confirmed by the micro-FTIR spectra of typical $(LSMO)_{0.8}(PPP)_{0.2}$, as displayed in figure 2. We find that the pellet calcined at 400 °C has the same wavenumber and relative intensity of IR peaks arising from PPP as the pellet that was not calcined. When the pellet is calcined at 500 °C, the main bands at 806, 1000, and 1482 cm^{-1} remain unchanged, but the band at 1600 cm^{-1} caused by C=C skeletal vibration of the benzene ring is weakened, demonstrating that the PPP has partly been broken.

Figure 3 shows XRD patterns of $(LSMO)_{1-x}(PPP)_x$ samples with $x = 0$, 0.2, 0.6, and 1. The patterns of the composites with $x = 0.2$ and 0.6 show two different sets of diffraction peaks, corresponding to LSMO rhombohedral perovskite and PPP phase respectively, which evidently indicates the coexistence of the two components.

Figure 4(a) presents a typical SEM image of $(LSMO)_{0.6}(PPP)_{0.4}$. The interfaces between PPP and LSMO can be clearly distinguished. The dark areas represent PPP and the light areas represent LSMO. The PPP powders are dispersed in a disordered fashion within the LSMO matrices. However, PPP congregations are not uniform in size. The observed size of PPP congregations ranges from hundreds of nanometres to a few microns. Though the combination of LSMO and PPP is not homogeneous, as shown by the micrographs, it can be considered that PPP particles are well distributed in LSMO matrices from the macroscopic viewpoint. Figure 4(b) displays a magnified image of the LSMO part. The crystallized LSMO particles are piled up closely, with polyhedral shapes, whose estimated size is in the range 100–150 nm.

Magnetic measurements show us that PPP is nonmagnetic over the entire detection temperature range. The Curie temperature (T_C) of LSMO measured at an applied field of 0.5 T is 365 K, close to that of the ceramic sample [19]. Figure 5 depicts the thermal dependence of the zero-field resistivity (ρ) and the MR value obtained at 5 T for composites with different x-values. The M–I transition temperature (T_{MI}) of the parent LSMO is about 305 K, apparently

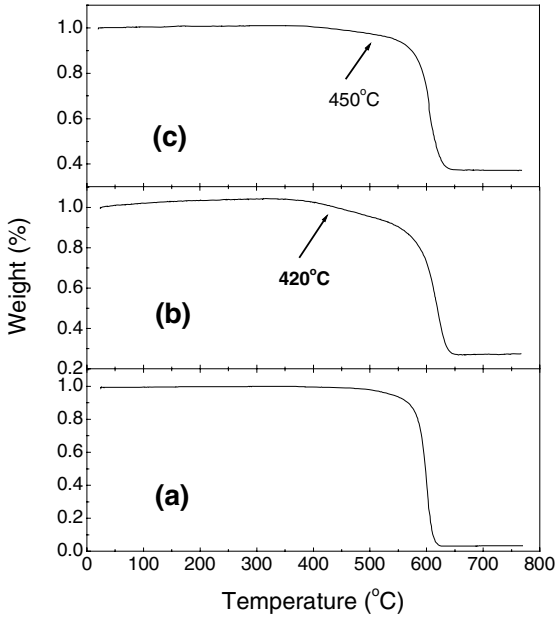

Figure 1. Thermal weight curves of $(LSMO)_{1-x}(PPP)_x$: (a) $x = 1$, (b) $x = 0.2$, and (c) $x = 0.6$.

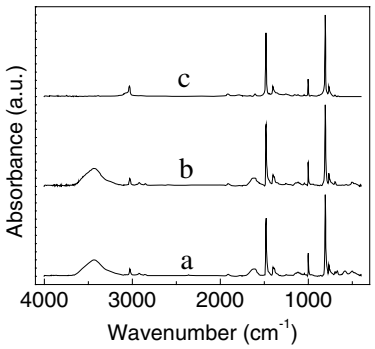

Figure 2. Micro-FTIR spectra of $(LSMO)_{0.8}(PPP)_{0.2}$ pellets: (a) without calcination, (b) calcined at 400 °C, (c) calcined at 500 °C.

lower than T_C. This is a characteristic feature caused by grain boundary (GB) effects in granular manganites due to the low connectivity between grains [17, 20]. On addition of PPP, the M–I transition becomes indistinct, accompanied with an increase in resistivity. When x goes up to 0.6, the composite behaves as an insulator. As we have found by measurement, the resistance of PPP is too large to be detected by our apparatus, indicating that PPP is in an insulating state in our case. PPP addition leads to the introduction of insulating regions in the composites. However, figure 5(b) clearly reveals that the MR of $(LSMO)_{1-x}(PPP)_x$ ($x = 0.1$–0.6) composites is enhanced compared with that of the parent LSMO from very low temperature even up to room temperature. In order to achieve further understanding of the regularity of the enhancement, we plot ρ and MR as functions of x at 5, 35, and 300 K in figure 6. It can be seen that the sharp increase in ρ occurs at $x = 0.1$ and 0.4. The value of ρ increases by almost two orders of magnitude when x varies from 0 to 0.1 and from 0.4 to 0.6.

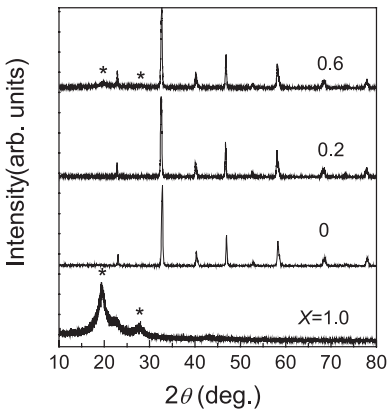

Figure 3. XRD patterns for $(LSMO)_{1-x}(PPP)_x$ with $x = 0$, 0.2, 0.6, and 1. The asterisks represent the diffraction peaks arising from PPP.

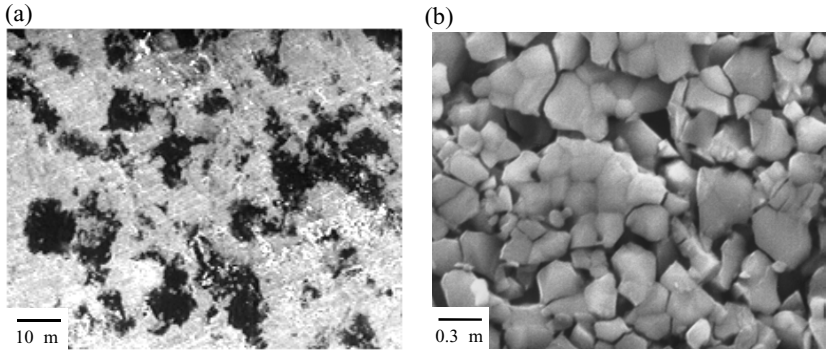

Figure 4. (a) A SEM micrograph of $(LSMO)_{0.6}(PPP)_{0.4}$ composite; (b) the magnified SEM image of the LSMO part in the same sample.

The x-dependences of MR at several temperatures shown in figure 6(b) indicate the maximal MR enhancement to be at $x = 0.2$. For instance, the MR for $x = 0.2$ is 54% at 35 K and 14% at 300 K, whereas the MR for $x = 0$ is 33% at 35 K and 10% at 300 K.

Furthermore, all the $(LSMO)_{1-x}(PPP)_x$ composites exhibit a remarkable low-field MR (LFMR) especially at low temperature, as displayed in figure 7(a). In the low-field region $H < 0.5$ T, a sharp rise in MR is observed, whereas the variation of the MR is nearly linear with a much smaller slope when the field is high enough. This LFMR behaviour is characteristically caused by granular LSMO [17]. In figure 7(b), we observe a similar field dependence of the magnetization (M). The experimental data for the MR are described well by the $(M/M_s)^2$ law in the low-magnetization region, showing a tunnelling MR [21]. On the other hand, M for $x = 0.1$ and 0.2 is much lower than that for LSMO. Because M for the composites originates from LSMO, we can calculate M for $x = 0.1$ and 0.2 according to M for the parent LSMO and its weight proportion in the composites. The calculated results are plotted as dashed lines, also in figure 7(b). Obviously, the experimental data are smaller than the as-calculated values. A similar phenomenon is also observed from 5 K up to room temperature in the M–T curves. Here, we can compare the magnetic moment per Mn ion (μ_{exp}) obtained under 5 T and at 5 K to achieve further understanding of the influence of PPP. The as-obtained μ_{exp} is 3.61 μ_B for

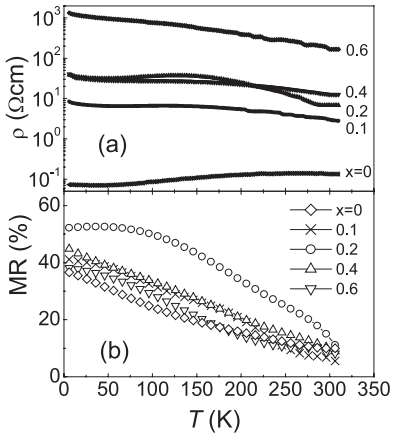

Figure 5. The temperature dependence of (a) the zero-field resistivity $\rho(T)$ and (b) the MR ratio over the whole temperature range for the $(\mathrm{LSMO})_{1-x}(\mathrm{PPP})_x$ series.

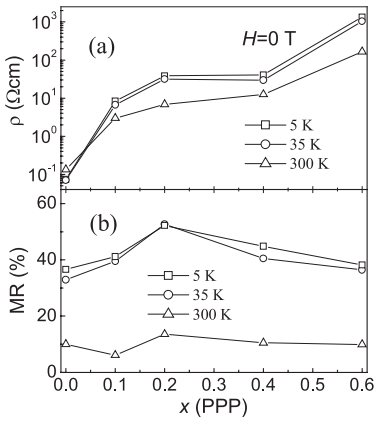

Figure 6. The influence of the PPP weight fraction x on (a) the resistivity and (b) the MR ratio at 5, 35, and 300 K.

$x = 0$, which agrees with the theoretical saturation magnetic moment of 3.67 μ_B, but μ_{exp} is 3.51 μ_B for $x = 0.1$ and 3.50 μ_B for $x = 0.2$. The difference in M and μ_{exp} between LSMO and LSMO/PPP leads us to take into account the extra magnetic disorder caused by PPP in the composites. The embedding of PPP into LSMO matrices not only dilutes the magnetization, but also results in additional magnetic disorder.

In our case, the magnetotransport is controlled by the spin-polarized electron tunnelling through the ferromagnetic nanosized LSMO grain boundaries. In the magnified SEM image of the LSMO region shown in figure 4(b), we see large numbers of discriminable LSMO particles. The above-mentioned observations, such as T_{MI} being lower than T_C, a broad M–I transition, the temperature-independent MR, and the striking LFMR, give us evidence that the GB effect plays an important role in the magnetotransport properties of the composites. As reported by others, the enhanced MR in the manganite composites is commonly interpreted within the framework of spin-polarized tunnelling [1–3]. The GBs of polycrystalline manganite and the introduced insulator layers when thin enough can act as tunnelling barriers. However, the

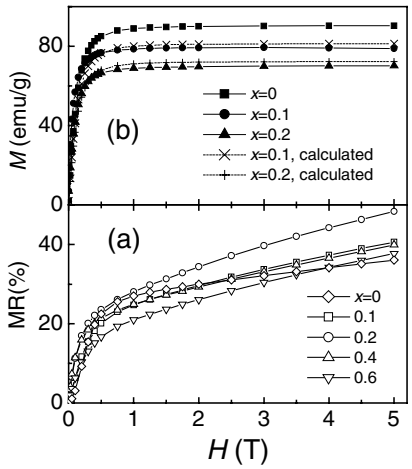

Figure 7. (a) The field dependence of the MR values for $(LSMO)_{1-x}(PPP)_x$ with various PPP weight fractions at 5 K. (b) The field dependence of the magnetization (M) for $x = 0$, 0.1, and 0.2 also at 5 K; the dashed curves represent M calculated according to the data for LSMO.

present LSMO/PPP composites are somewhat different. From the typical SEM micrograph shown in figure 4, we find that PPP powders are congregated as large particles, making it impossible for the insulating PPP layers to directly act as tunnelling barriers between the LSMO grains. Nevertheless, the magnetic measurement in figure 5 shows additional magnetic disorder caused by PPP. We suggest that the additional magnetic disorder should arise from two scenarios. First, the polymer PPP has a softening temperature of around 400 °C as depicted by figure 1, which makes it easy for dispersal across the GBs of LSMO to occur. Thereby, the addition of PPP gives rise to contamination at the LSMO surfaces and hence enhancement of the GBs. In other words, PPP leads to enhanced spin disorder at the surfaces of LSMO particles, especially in the region neighbouring the PPP. Secondly, for the pellets of the composites finally calcined at 400 °C, the redox reaction between PPP and the oxygen atoms that had escaped from the LSMO lattices is not negligible, and, as a consequence, inhomogeneous oxygen vacancies appear spontaneously in the composites. These random vacancies will possibly result in disordered structure and hence magnetic inhomogeneity [22]. Here, the magnetic disorder caused by PPP gives the crucial contribution to the MR enhancement. When a field is applied, the spins within this disordered region realign along the field direction, leading to an enhanced rate of electron tunnelling between LSMO grains.

4. Conclusions

We have introduced a polymer component, PPP, into CMR manganite matrices. With calcining at 400 °C, PPP can exist stably in the LSMO/PPP composites. Significantly enhanced MR effects from low temperature up to room temperature are observed in the LSMO/PPP composites. The enhancement strongly depends on the PPP content, which can be mainly attributed to the intergrain spin-polarized tunnelling. Moreover, the magnetic disorder caused by PPP could provide an additional contribution to the enhanced MR. These results reveal an opportunity to improve MR properties by combining hole-doped manganites with special polymers.

Acknowledgments

The authors would like to acknowledge the support of the MOST (G19980613), the NSFC (29831010, 20023005), and the Founder Foundation of PKU.

References

[1] Balcells Ll, Carrillo A E, Martinez B and Fontcuberta J 1999 *Appl. Phys. Lett.* **74** 4014
[2] Petrov D K, Krusin-Elbaum L, Sun J Z, Field C and Duncombe P R 1999 *Appl. Phys. Lett.* **75** 995
[3] Gupta S, Ranjit R, Mitra C, Raychaudhuri P and Pinto R 2001 *Appl. Phys. Lett.* **78** 362
[4] Liu J M, Yuan G L, Sang H, Wu Z C, Chen X Y, Liu Z G, Du Y W, Huang Q and Ong C K 2001 *Appl. Phys. Lett.* **78** 1110
[5] Hwang H Y, Cheong S W, Ong N P and Batlogg B 1996 *Phys. Rev. Lett.* **77** 2041
[6] Yan C H, Xu Z G, Zhu T, Wang Z M, Cheng F X, Huang Y H and Liao C S 2000 *J. Appl. Phys.* **87** 5588
[7] Huang Y H, Wang S, Luo F, Wang Z M, Liao C S and Yan C H 2002 *Chem. Phys. Lett.* **362** 114
[8] Yan C H, Luo F, Huang Y H, Li X H, Wang Z M and Liao C S 2002 *J. Appl. Phys.* **91** 7406
[9] Huang Y H, Yan C H, Luo F, Song W, Wang Z M and Liao C S 2002 *Appl. Phys. Lett.* **81** 76
[10] Li X H, Huang Y H, Yan C H and Wang Z M 2002 *Appl. Phys. Lett.* **81** 307
[11] Nazar L F, Zhang Z and Zinkweg D 1992 *J. Am. Chem. Soc.* **114** 6239
[12] Beecroft L L and Ober C K 1999 *Chem. Mater.* **9** 1302
[13] Cao G, Garcia M E, Aleala M, Burgess L F and Mallouk T E 1992 *J. Am. Chem. Soc.* **114** 7574
[14] Huang Y H, Chen X, Wang Z M, Liao C S and Yan C H 2002 *J. Appl. Phys.* **91** 7733
[15] Kovacic P and Kyriakis A 1963 *J. Am. Chem. Soc.* **85** 454
[16] Kovacic P and Koch F W 1963 *J. Org. Chem.* **28** 1864
[17] Huang Y H, Xu Z G, Yan C H, Wang Z M, Zhu T, Liao C S, Gao S and Xu G X 2000 *Solid State Commun.* **114** 43
[18] Kovacic P and Oziomek J 1964 *J. Org. Chem.* **29** 100
[19] Urushibara A, Moritomo Y, Arima T, Asamitsu A, Kido G and Tokura Y 1995 *Phys. Rev.* B **51** 14 103
[20] de Andrés A, García-Hernández M and Martínez J L 1999 *Phys. Rev.* B **60** 7328
[21] Coey J M D 1999 *J. Appl. Phys.* **85** 5576
[22] Blasco J, García J, de Teresa J M, Ibarra M R, Perez J, Algarabel P A and Marquina C 1997 *Phys. Rev.* B **55** 8905